PERGAMON

Journal of the Mechanics and Physics of Solids
48 (2000) 621–648

JOURNAL OF THE
MECHANICS AND
PHYSICS OF SOLIDS

www.elsevier.com/locate/jmps

Micromechanical simulation of the failure of fiber reinforced composites

Chad M. Landis[a,*], Irene J. Beyerlein[b], Robert M. McMeeking[c]

[a]*Division of Engineering and Applied Science, Harvard University, Pierce Hall, Cambridge, MA 02138, USA*

[b]*Materials Science and Technology Division, Los Alamos National Laboratory, Los Alamos, NM 87545, USA*

[c]*Department of Mechanical and Environmental Engineering, University of California, Santa Barbara, CA 93106, USA*

Received 1 February 1999; received in revised form 5 July 1999

Abstract

The strength of unidirectionally reinforced fiber composites is simulated using the three dimensional shear lag model of Landis, C. M., McGlockton, M. A. and McMeeking, R. M. (1999) (An improved shear lag model for broken fibers in composites. J. Comp. Mat. 33, 667–680) and Weibull fiber statistics. The governing differential equations for the fiber displacements and stresses are solved exactly for any configuration of breaks using an influence superposition technique. The model predicts the tensile strength of well bonded, elastic fiber/matrix systems with fibers arranged in a square array. Length and strength scalings are used which are relevant for elastic, local load sharing composites. Several hundred Monte Carlo simulations were executed to determine the statistical strength distributions of the composite for three values of the fiber Weibull modulus, $m = 5$, 10 and 20. Stress–strain behavior and the evolution of fiber damage are studied. Bundle sizes of 10×10, 15×15, 20×20, 25×25, 30×30 and 35×35 fibers of various lengths are investigated to determine the dependence of strength on the composite size. The validity of weakest link statistics for composite strength is examined as well.

* Corresponding author.
E-mail address: landis@esag.harvard.edu (C.M. Landis).

0022-5096/00/$ - see front matter
PII: S0022-5096(99)00051-4

Keywords: B. Fiber-reinforced composite material; A. Stress concentrations; Fracture mechanisms; C. Probability and statistics; Shear lag

1. Introduction

Structural fiber composites exhibit considerable variation in their tensile strength depending on the type of fiber reinforcement and matrix material. The tensile strength exhibits a dependence on the size of the composite, with the median strength of larger composites being weaker than that of smaller ones. This behavior is commonly termed "size effect". The characteristics of the statistical strength distribution and severity of this size effect depend on the constituent material properties and microstructure.

Reliability concerns in utilizing fiber composites in structural applications has motivated the development of many numerical and analytical statistical strength models. These models are needed to predict the dominant failure modes and statistical strength distributions of the composite based on the statistical fiber strength, interface and matrix properties and specimen dimensions. The strength of such composites depends on the evolution of damage, which is a combination of fiber fracture, matrix cracking, debonding and inelastic matrix deformation, throughout the application of loading. The focus of our computational modeling will be to determine the initiation and linking of fiber fractures as a result of the interplay between fiber stress concentrations and the statistical variation in fiber strength.

Most of the earlier analytical strength models use idealized load sharing rules, such as nearest neighbor local load sharing, global load sharing (GLS) or equal load sharing, and some parametric form of the Weibull distribution to describe fiber strength. To extrapolate to longer composite lengths and bundle sizes, asymptotic analyses and weak link scalings are used. Exact probability calculations for even the simplest of local load sharing rules are enormously difficult except for small numbers of fibers, $n < 10$, see Harlow and Phoenix (1978a,b). Significant results from this idealized modeling work are that cumulative progression of fiber fractures lowers variation in composite strength thereby reducing the size effect of the composite relative to that of the fibers, and the distribution for the composite strength is not Weibull.

More sophisticated mechanical models are required to calculate stress redistribution without the use of ad hoc local load sharing rules. Finite element analysis (FEA) is probably the best candidate for determining the complex stress and strain states in the fibers and matrix. However, to date only the six nearest neighbors around a fiber with a single break have been analyzed using FEA, Nedele and Wisnom (1994). Furthermore, using FEA to analyze arbitrary configurations of breaks including progressive fiber failure would require excessive computation, and hence has not been attempted.

With the use of the shear lag assumption, that fibers can be modeled as one dimensional structures, many computational difficulties can be overcome while maintaining the essential physics of load transfer. Multiple fiber shear lag models replace the exact governing partial differential equations for the composite with an approximate, but mechanically justifiable, set of coupled ordinary differential equations. For a survey of shear lag models see Landis and McMeeking (1999). Shear lag models have been used successfully to explain many load transfer mechanisms in fiber composites. Some of the mechanisms investigated with shear lag models include viscoelasticity in the matrix, the effects of axial matrix stiffness, fiber/matrix interface sliding, and non-uniform fiber spacing (Beyerlein and Landis, 1999; Beyerlein and Phoenix, 1996; Beyerlein et al., 1998; Landis and McMeeking, 1999). Results of these shear lag models agree with the observations, e.g. Van den Heuvel et al. (1996), that increases in the axial stiffness of the matrix and increased amounts of interface sliding, decrease stress concentrations in fibers neighboring broken fibers.

As opposed to analytical modeling which requires very simple fiber break configurations, numerical simulation has the advantage of accounting for interactions of multiple fiber breaks as they accumulate up to failure. Some pioneering work in coupling shear lag analysis and Monte Carlo simulation include Beyerlein and Phoenix (1997a,b) and Ibnabdeljalil and Curtin (1997). Beyerlein and Phoenix (1997a) used the two dimensional shear lag model of Hedgepeth (1961), along with the simplification that fiber breaks could only occur along a single plane. In contrast, Ibnabdeljalil and Curtin allowed for staggered break configurations in a three dimensional fiber array but used the approximate stress analysis technique of Zhou and Curtin (1995) to account for interactions between non-planar breaks. To their credit, both works developed analytical probability models for the distribution of composite strength which achieved good agreement with their simulation results. In this paper, we will allow arbitrary three dimensional configurations of breaks to occur in a square array of fibers and we will solve the governing shear lag equations *exactly*.

The elastic shear lag analysis in this work falls under the general theme of local load sharing (LLS), wherein fibers can fail due to concentrated stresses near previously broken fibers. Employing the shear lag model used in this work, Landis and McMeeking (1999) showed that the global to local load sharing spectrum can be parameterized by the quantity $\sqrt{E_f/G_m}\tau_0/\sigma_{max}$, where G_m is the shear modulus of the matrix, τ_0 is the shear sliding resistance of the fiber/matrix interface, and σ_{max} is the strength of the composite. It was demonstrated that as $\sqrt{E_f/G_m}\tau_0/\sigma_{max}$ approaches zero, the GLS limit, with no stress concentrations on intact fibers and linear stress recovery from a break along a broken fiber, is obtained. Noteworthy works on the strength of GLS composites include the approximate models of Curtin (1991a,b) and Neumeister (1993), the exact solution given by Hui et al. (1995) for infinite GLS composites and Phoenix et al. (1997) on size effects. In GLS, stress transfer around broken fibers is governed entirely by sliding at the fiber/matrix interface. In this work, we will simulate composite failure at the LLS end of the load sharing spectrum, i.e. $\sqrt{E_f/G_m}\tau_0/\sigma_{max} > 0.47$, as shown in Landis

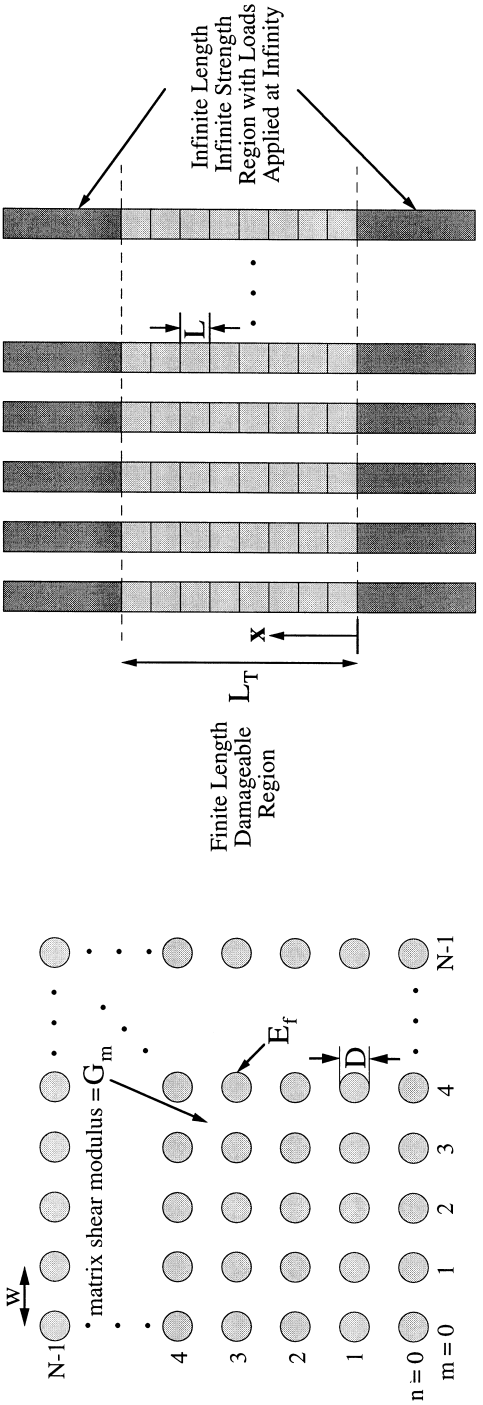

Fig. 1. Top and side views of the composite. The fibers are arranged in a square array and the coordinate along the fiber direction is x.

and McMeeking, where stress transfer is governed entirely by the elasticity of the fibers and matrix.

We will analyze the composite size effect separately in length and in fiber bundle size, introduce an efficient scheme for properly assigning flaws along fibers and study the composite stress–strain behavior and fiber damage evolution as they are related to the fiber strength statistics. The concept of a minimum scaleable weak link composite volume is investigated in detail. Lastly, the predictive capability of the model is tested against experimental strength measurements on impregnated fiber tows, in which the agreement is favorable.

2. Stress analysis

2.1. Model geometry and governing equations

The shear lag model of Landis et al. (1999) and an influence superposition technique are used for the stress analysis around multiple fiber breaks. Fig. 1 is a schematic of the geometry of the composite to be modeled. The fibers lie parallel to the x direction and are arranged uniformly in a square array. Each fiber can be located in the array by an integer pair (m, n). A finite $N \times N$ array of fibers is shown, where N is the number of fibers along the m and n directions and m and n range from 0 to $N-1$. In order to study failure, only a finite number of fibers and failure sites can be considered; as Fig. 1 shows, there is a finite length, L_T, along the fibers within which breaks are permitted. The spacing between fibers is w, the fiber diameter is D, and the fiber cross-sectional area is $\pi D^2/4$. The fibers are assumed to be well bonded to the matrix and the matrix is unable to carry any axial loads, i.e. the axial modulus of the matrix, E_m, is zero but the shear modulus, G_m, is finite. This is a standard shear lag assumption and is justifiable due to cracking of ceramics, yielding of metals, and the low modulus of polymers and epoxies which cause these matrix materials to be ineffective for supporting axial loads in comparison to the high modulus, high strength fibers. Hence, the primary role of the matrix is to transfer loads between fibers via shear stresses. It is also assumed that it is reasonable to neglect the transverse displacements of the fibers.

As described in Landis et al. (1999) the governing differential equations for this shear lag model are

$$\begin{aligned}&\frac{d^2 u_{m,n}}{d\xi^2} + u_{m+1,n+1} + u_{m+1,n} + u_{m+1,n-1} + u_{m,n+1} + u_{m,n-1} + u_{m-1,n+1}\\&\quad + u_{m-1,n} + u_{m-1,n-1} - 8u_{m,n}\\&\quad = 0\end{aligned} \tag{1}$$

where the normalized spatial coordinate is

$$\xi = \sqrt{\frac{4}{3\pi}}\sqrt{\frac{G_{\mathrm{m}}}{E_{\mathrm{f}}}}\frac{x}{D} \tag{2}$$

and the normalized fiber displacement is

$$u = \sqrt{\frac{4}{3\pi}}\sqrt{\frac{G_{\mathrm{m}}}{E_{\mathrm{f}}}}\frac{1}{\varepsilon}\frac{U}{D} \tag{3}$$

where x is the axial coordinate along the fibers, $U_{m,n}$ is the axial displacement of fiber $(m,\ n)$ and is a function of x only and ε is the strain applied to the composite. Note that in this model there is no dependence on the fiber spacing w. This results due to the assumptions that the matrix has no axial stiffness and transverse displacements are neglected. The fact that w does not appear, can be understood by noting that the shear stiffness per unit thickness of a square slab of matrix material does not depend on the length of a side of the square and is exactly equal to G_{m}. The normalized Hooke's law and compatibility condition for the fibers are

$$\frac{\sigma_{m,\ n}}{E_{\mathrm{f}}\varepsilon} = \frac{\varepsilon_{m,\ n}}{\varepsilon} = \frac{\mathrm{d}u_{m,\ n}}{\mathrm{d}\xi} \tag{4}$$

where $\sigma_{m,n}$ and $\varepsilon_{m,n}$ are the axial stress and strain in fiber $(m,\ n)$.

2.2. Influence superposition technique

An influence superposition technique is used to solve Eq. (1) for complex, non-planar arrangements of traction free breaks, e.g. Sastry and Phoenix (1993) and Landis and McMeeking (1999). In this section, we will present only the significant details of the method. The necessary building blocks for influence superposition are the solutions for a single break in one fiber and no breaks in all other fibers. The influence functions $q_{m,n}(\xi)$ give the amount of stress present in fiber $(m,\ n)$ at position ξ due to a unit opening load applied at $(m = 0,\ n = 0,\ \xi = 0)$. The procedure used to solve for the influence functions is given in the Appendix.

Assume that there are M fiber breaks located at positions $(m_i,\ n_i,\ \xi_i)$, $i = 1$ to M. Let Λ_{ij} be the amount of stress added at break i due to a unit opening load at break j; then

$$\Lambda_{ij} = q_{|m_i - m_j|,\ |n_i - n_j|}(|\ \xi_i - \xi_j\ |). \tag{5}$$

Note that the matrix with components Λ_{ij} is fully dense, symmetric and negative definite. To obtain the solution for traction free breaks and far field applied strain, the problem of unit opening loads applied at each break under zero far field strain must first be solved. The following set of linear algebraic equations is solved to obtain this solution

$$\sum_{j=1}^{M} \Lambda_{ij} w_j = -1 \tag{6}$$

for all i, $i = 1$ to M, where the w_j are weights, and the product $w_j u^{\text{open}}$ gives the crack opening displacement of the jth break, and u^{open} is the crack opening displacement of a single break subjected to a unit opening load (see Appendix). The final solution for the fiber stresses at any location with M arbitrarily located traction free breaks with a uniform far field applied strain, ε, is

$$\frac{\sigma_{m,\,n}(\xi)}{E_f \varepsilon} = 1 + \sum_{j=1}^{M} w_j q_{|m-m_j|,\,|n-n_j|}(|\,\xi - \xi_j\,|). \tag{7}$$

Within the failure simulations, it is assumed that only a finite length of fibers L_T is able to sustain damage. In order to calculate a stress–strain curve for the composite, the average strain in the damageable region (i.e. $0 < x < L_T$) is required. Using Hooke's law for the relationship between fiber stress and strain,

	-2	*-1*	*m=0*	*1*	*2*
2	**1.0058**	**1.0094**	**1.012**	**1.0094**	**1.0058**
	1.054	0.92	0.863	0.92	1.054
1	**1.0094**	**1.076**	**1.081**	**1.076**	**1.0094**
	0.92	0.476	0.491	0.476	0.92
n=0	**1.012**	**1.081**	**SCF 0**	**1.081**	**1.012**
	0.863	0.491	PAL 0	0.491	0.863
-1	**1.0094**	**1.076**	**1.081**	**1.076**	**1.0094**
	0.92	0.476	0.491	0.476	0.92
-2	**1.0058**	**1.0094**	**1.012**	**1.0094**	**1.0058**
	1.054	0.92	0.863	0.92	1.054

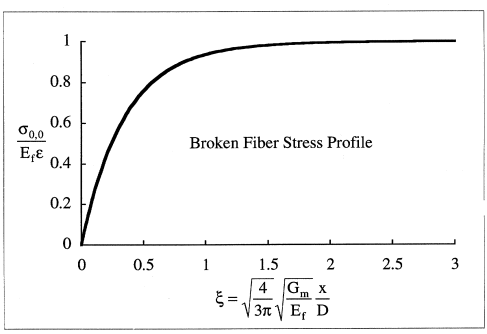

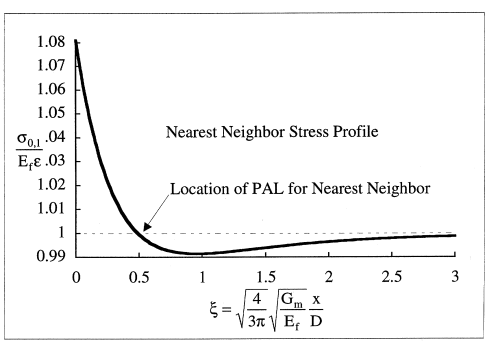

Fig. 2. (a) The stress concentration factors (SCF) and positively affected lengths (PAL) predicted by the shear lag model for a single fiber break. The position $m = 0$, $n = 0$ represents a single broken fiber with zero stress on the break plane. The bold, top number is the SCF on the plane of the break for that fiber and the lower number is the PAL. (b) The stress profiles along a broken and nearest neighbor fiber as predicted by the shear lag model.

equilibrium of force between parallel planes, and the appropriate normalizations, it can be shown that the average strain in the composite, $\bar{\varepsilon}$, is

$$\bar{\varepsilon} = \varepsilon\left[1 + \frac{1}{N^2\hat{L}_{\mathrm{T}}}\sum_{i=1}^{M} w_i u^{\mathrm{open}}\right] \tag{8}$$

where ε is the strain applied to the fibers at infinity, w_i is the weight function for the ith break, and the normalized length of the damageable region is

$$\hat{L}_{\mathrm{T}} = \sqrt{\frac{4}{3\pi}}\sqrt{\frac{G_{\mathrm{m}}}{E_{\mathrm{f}}}}\frac{L_{\mathrm{T}}}{D} \tag{9}$$

Fig. 2(a) is a schematic of the in-plane stress concentration factors and positively affected lengths predicted by Eq. (1) for an infinite square array of fibers with a single break. Fig. 2(b) contains the corresponding distributions of the axial stress along the broken and nearest neighbor fibers.

3. Flaw statistics

Eqs. (1)–(7) allow the calculation of the axial stress along any fiber (m, n) in the composite, but these equations say nothing about where and at what stress the fiber breaks will occur. Unlike the stress analysis model, the statistical model requires discretization of all fibers within $0 < x < L_{\mathrm{T}}$. The assignment of discrete failure sites to represent a continuous description of statistical strengths is not a trivial task. In this section, an efficient scheme for assigning flaw locations, which leads to convergent composite strengths, is introduced. The strengths of these potential failure sites are assumed to follow a Weibull distribution, but in principle, any statistical distribution can be incorporated into this model.

As shown in Fig. 1, an $N \times N$ array of fibers is considered and a finite number of flaws are distributed along the fibers. Each fiber with total length L_{T} is divided into N_{Z} segments of length L such that $N_{\mathrm{Z}}L = L_{\mathrm{T}}$. We assume that every segment of fiber is independent and identically distributed Weibull. Therefore, a length L of a fiber segment loaded to stress σ has a probability of failure, $\hat{P}_{\mathrm{f}}$,

$$\hat{P}_{\mathrm{f}} = 1 - \exp\left[-\frac{L}{L_0}\left(\frac{\sigma}{\sigma_0}\right)^m\right] \tag{10}$$

where L_0 and σ_0 are the Weibull length and strength parameters and m is the Weibull modulus. In order to reproduce a composite consisting of Weibull fibers, each fiber segment is assigned a strength

$$\sigma_i^{\max} = \sigma^*\left(\frac{1}{\hat{L}}\right)^{1/m}\left[\ln\left(\frac{1}{1-\delta_i}\right)\right]^{1/m} \tag{11}$$

where

$$\hat{L} = \sqrt{\frac{4}{3\pi}}\sqrt{\frac{G_{\mathrm{m}}}{E_{\mathrm{f}}}}\frac{L}{D} \tag{12}$$

and

$$\sigma^* = \sigma_0\left(\sqrt{\frac{4}{3\pi}}\sqrt{\frac{G_{\mathrm{m}}}{E_{\mathrm{f}}}}\frac{L_0}{D}\right)^{1/m}. \tag{13}$$

ln denotes the natural logarithm, $\sigma_i^{\max}$ is the strength of the ith fiber segment and δ_i is a uniform deviate produced by a random number generator such that $0 < \delta_i < 1$. The parameter $\hat{L}$ is the normalized fiber segment length and σ^* is the composite strength scaling, originally proposed by Landis and McMeeking (1999) for determining failure probabilities in fibers neighboring breaks. Eqs. (12) and (13) represent the appropriate length and strength scalings for the well bonded, local load sharing composite systems analyzed in this model. In the simulations, σ^* is a material property of the composite system and $\hat{L}$ is the discretization size which must be chosen to be small enough to minimize discretization errors. The position of the single failure site within a given segment will be chosen in two ways: (i) at random under the assumption that the locations of the flaws are distributed uniformly within the segments, or (ii) to be placed in the middle of each segment. The latter, method (ii), is the common method of previous works. Both of these assumptions will be investigated in this work, with scheme (i) proving to be the more efficient method, allowing longer segment lengths $\hat{L}$ for the same accuracy.

4. Simulation algorithm

Prior to any simulations, Eq. (1) must be solved for a given $N \times N$ fiber bundle size, as described in detail in the Appendix. Once the solution is obtained, all of the influence functions, $q_{m,n}$ for $m, n = 0$ to $N-1$, are stored for values of ξ from 0 to 12 at intervals of $\Delta\xi = 0.1$. In order to obtain the influence function for any arbitrary value of ξ, linear interpolation is used between the nearest stored values.

All of the Monte Carlo simulations are run by controlling the average strain in the damageable region. Initially all fibers are intact when the applied stress and average strain in the system are zero. The weakest fiber segment is identified and the average strain is incremented such that only that segment fails. The solution to Eq. (6) for a single fiber break, $M = 1$, is obtained and Eq. (7) is used to calculate the stress at all of the intact failure sites. If any of the failure sites are overloaded then the *most* overloaded site is found. Only the most overloaded site is broken and Eq. (6) is solved again, now for multiple breaks. In order to maintain a constant average strain in the damageable region during this step, the far field

applied stress is decreased. If there are still overloaded sites then the previous step is repeated, one break at a time, until all intact sites have strengths greater than the current axial stresses at those sites.

Once this equilibrium configuration of breaks is obtained, the average strain in the damageable region must be incremented in order to cause further damage. The strain increment required to break each intact site is calculated and the site with the smallest required increment is the next site to break. Note that this is not necessarily the weakest intact site. The average strain in the damageable region is incremented by this amount and the appropriate failure site is broken. The procedure of finding an equilibrium configuration of breaks at each increment is repeated until, as a result of a large accumulation of fiber breaks, the far field applied stress has dropped a significant amount below the maximum value that had been obtained during all of the previous steps. At this point, the maximum value is defined as the ultimate strength and the simulation is terminated.

After each break, i.e. the Mth break, the size of the matrix that must be inverted in Eq. (6) increases by one. Since the inverse of the previous $(M-1)\times(M-1)$ matrix is known, an inversion by partitioning scheme, as described by Press et al. (1992), is used. This procedure reduces the inversion process from an order M^3 operation to an order M^2 operation.

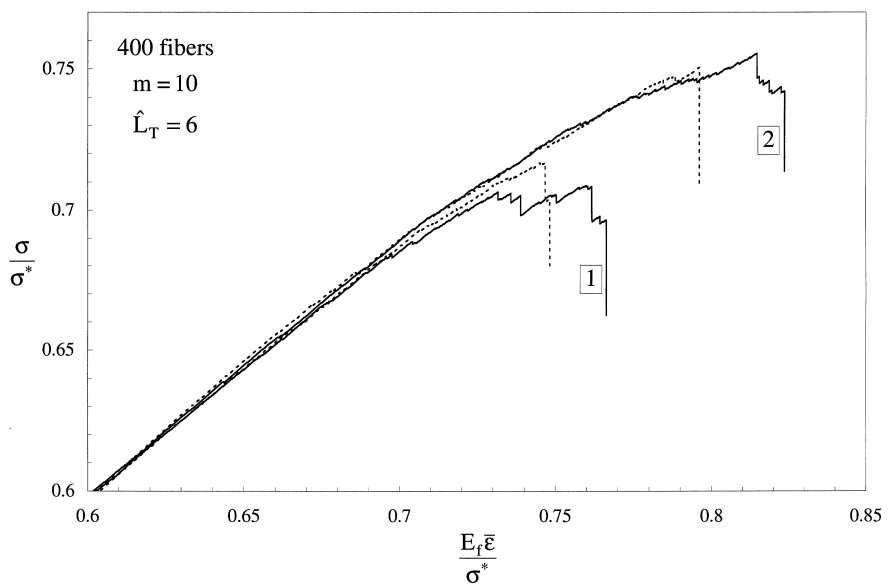

Fig. 3. Four stress–strain curves, two strong and two weak, from the strength distribution for 400 fibers, $m = 10$ and $\hat{L_T} = 6$.

5. Results

Five hundred to 1000 Monte Carlo simulations were run for various composite sizes and fiber Weibull moduli. For each simulation the ultimate stress $\sigma_{\max}$, strain to failure, number of breaks at failure and final failure plane were recorded. For each set of similar simulations, the ultimate strengths were ranked to produce statistical strength distributions. Also, for a few selected simulations, the composite stress–strain curves were recorded. For the stress–strain curves presented below, the length of each fiber segment was chosen to be $\hat{L}=0.25$. The appropriateness of this value of $\hat{L}$ will be discussed in greater detail when the strength distributions are presented.

Failure Pattern 1

	13						12		2				3		9			15	
						3	7			1					4	5	6		8
3					9			0	7	-2	-1				4	5			
15		-1	0				12	-1	0	18		9							
3			15					0	0	0	13		-1		1	-4			
19				14			1	-1	0	0	-2	-3	-2		3			2	
	0		3			-3	0	0	0	0	0	-1	-1						
				17		-3	1	0	0	0	0	0	-3						
		11		1		0	0	1	0	0	0	0	-2	1	-4	4			6
			2	3			-1	1	0	1	0	0	-3	-4	-3				9
		12		18		-2	-3	-2	1	0	-1	-2			-3	4	5		
1					-3	-2	-2	-3	-2										
	-3		18			3	-3	-2	-4			-4						10	
19		4			-3	1	-3	-1			-4		14		8		9	11	
	-1		-1					-2		3	17	2	3			16			
-1	17	-1		-4					11	4		-3					-2	1	16
-2	17					-3	9		3	-4			19	12				-2	
		15	17				10				5					-1		-2	
					4		-2								4	2	1		
		-3			-1		5								18				

Fig. 4. The distribution of breaks at the peak stress level for the stress–strain curve labeled 1 in Fig. 3. Each box represents a fiber and each number represents a break along that fiber. The numbers denote the plane at which the fiber has broken, a zero represents the final failure plane, 1 is a break on the plane above the failure plane, −1 is one plane below and so forth.

5.1. Stress–strain curves and failure patterns

As discussed in the Simulation Algorithm section, all of the simulations were run by controlling the average strain in the damageable region. Fig. 3 is a set of stress–strain curves for a composite with a fiber Weibull modulus of 10, a 20×20 fiber bundle, and $\hat{L}_T = 6$. Four curves are shown, two weak simulations and two strong simulations representing four different distributions of flaw sizes. Note that the stress reported on the ordinate of this plot is the stress in the fibers, not the stress in the composite. In order to obtain the composite stress, one must multiply the fiber stress by the fiber volume fraction. The stress–strain curves shown, and all others created by this model, consist of a series of upwardly sloping straight lines, along which no breaks occur, connected by vertical segments of constant

Failure Pattern 2

-4	6						12	0		2	2	-8	4	-8		-1	-2		0
		12	9	7	-3	-2			1	2	-2	7	10						
	-7	-2	5		9						5	3	3			10			-5
		-7			-3	10					6		0	2			2		8
7				9	10	4	4	7		-2	6					-8	15		
			14		10		4				5				8	0	11	7	
	9	6	8	10		4		10	9	-7	-6						5		
4		-2						4		-6		12	-6		4	7	7	7	
			6	6			10				-6	-7			-1	-4	-2		
-6	-6			5	-1				5		-7	3							
12				11			7		0	10	-8	0	10	6		5			1
	13	-7		-2	-1		1		10	10	1	3		11	5		-1	10	
2				-1	-1		5	-7			8		10	5		4		3	2
3				7	-1			12	3				0	10		1	1		
14	0			-7	11	-7		-3			2	4		3				-5	
			1	-3	11	5	6	-3	0	-1		2	2	2	-3	2			-6
-7	-1				6	6					8		-5		-2		-5		
-2	-1	6	6	1			12	12		-1		2	0	1		-5		-2	2
12					4	4						4							
	10			-8	-8	-7		-5		6	-5		4	12		-5	11		

Fig. 5. The distribution of breaks at the peak stress level for the stress–strain curve labeled 2 in Fig. 3. Each box represents a fiber and each number represents a break along that fiber. The numbers denote the plane at which the fiber has broken, a zero represents the final failure plane, 1 is a break on the plane above the failure plane, -1 is one plane below and so forth.

average strain during which fiber breakage develops. The slope of each non-vertical segment multiplied by the fiber volume fraction is the Young's modulus for a composite with the prevailing amount of damage.

Figs. 4 and 5 represent the distribution of breaks in the composite just prior to failure, i.e. at $\sigma_{\max}$. Fig. 4 is the distribution for the stress–strain curve marked 1 in Fig. 3 and Fig. 5 corresponds to the number 2 curve. The charts in Figs. 4 and 5 are schematics of a cross-section of the composite in and around the failure plane. Each square represents a fiber. Each number in a square represents a fiber break, giving the approximate x-coordinate (see Fig. 1) of the break location. The approximate distance of a given break from the final failure plane would be the number reported in the square times the normalized segment size $\hat{L}$. A zero represents the final failure plane, 1 is a break on the plane above the failure plane, -1 is one plane below and so forth. It is possible for fibers to have multiple breaks, but only the break nearest to the final failure plane is reported. Breaks that are most likely to link up for the final separation of the composite are shaded gray and used to deduce the ultimate failure plane. Other notable clusters of breaks removed from the failure plane have bold outlines.

There is a distinct difference between the pattern of breaks of Fig. 4 for the weak composite and the pattern of Fig. 5 for the strong composite. The weak pattern has a very large cluster of breaks with some distributed single breaks but

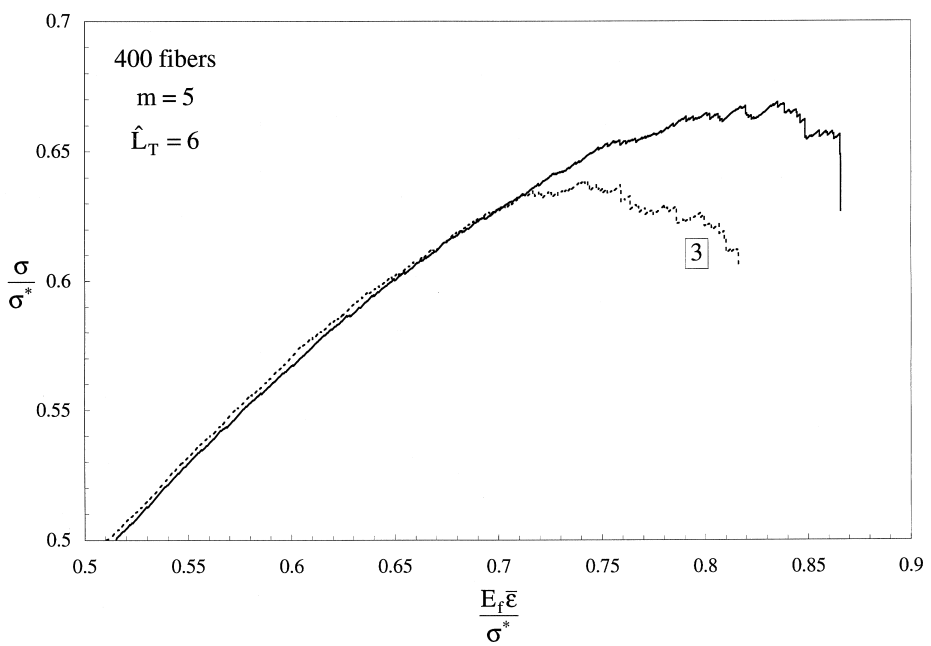

Fig. 6. Two stress–strain curves, one strong and one weak, from the strength distribution for 400 fibers, $m = 5$ and $\hat{L}_T = 6$.

very few out of plane clusters. In contrast to Fig. 4, the pattern of breaks for the strong specimen contained no large clusters, and as shown in Fig. 5, many of the other planes in the composite also contained small clusters of breaks.

Fig. 6 contains two stress–strain curves from the simulations with bundles of 20×20 fibers with $\hat{L_T} = 6$ and $m = 5$. Notice that the relative strength is lower for $m = 5$ than for $m = 10$ and the $m = 5$ stress–strain curves deviate more from linear behavior than the $m = 10$ curves. This "softness" in the material is due to the variability of the fiber strengths. At stresses below failure, fiber bundles with $m = 5$ contain more breaks than bundles with $m = 10$ fibers. These breaks each have a crack opening displacement that enhances the strain in the composite and effectively makes the composite more compliant. Fig. 7 is the failure pattern corresponding to stress–strain curve 3 of Fig. 6. Again, this chart represents the distribution of breaks at the peak stress. The most significant difference between

Failure Pattern 3

14			-3			8	4	3			3	2		3		6		12	
10	12	0	-4	-3	7	10	-2		11	2	2	5	2	2	5				2
9	-8	-4	5	8		-5	-3		4		-7	2		-2	2	10	-5		
0		0	-1	0	-6	3		0	-4	-3	4	-5	4		-3	-1	10	1	
	0	-5	7	1	3	-1	-7	1	7	6	3		3	-2					10
		12			-1	-7	0			0	-3		0	4	7	-3	-2		5
3		5	4	7			0	-1	-7	-1	1	0		-2		-3	14	-8	-2
		1	0	3	-9			4	-1		5	-4	-2	-1	-8	0	-6		6
1	3	5	3		0	1		-6	7	3	-8		-2	-1	0	1		1	13
5	-3			1	-8				5	4		10		6	6	1		-2	0
		14	9	0	9	12			9	0	7		6			13			14
	-5	5	0		-1		13	13	3				-3						
-4	7	2	1	6	11	-7	-5		7		-8		-8		7			8	5
12		0			11	12			7	6	12	10	11		8	-6	1		
-5	-2							2	0					10	-8	1			
2						3	6		13	14	10	0	11						14
6	13		3	1			11			7	13	11		0	-9		3	-1	2
-4		0	0	2	2	9	7	5	7	9		-1		3		4	9	-1	-6
-3	-1		0	1	-9	0	10		2	9	10	1		12				14	
-4		-1		-2	4	10	13		4	8	14	-1		12			-1	0	-7

Fig. 7. The distribution of breaks at the peak stress level for the stress–strain curve labeled 3 in Fig. 6. Each box represents a fiber and each number represents a break along that fiber. The numbers denote the plane at which the fiber has broken, a zero represents the final failure plane, 1 is a break on the plane above the failure plane, -1 is one plane below and so forth.

the failure patterns from composites with fiber Weibull modulus of 5 and 10 is that there is much more distributed damage in the composites with $m = 5$. Unlike the weak sample from the $m = 10$ simulations, failure pattern 3 does not have a distinct crack or large concentrated cluster of breaks. Instead, within the small clusters found on pattern 3 there tend to be strong fibers that are bridging the cracks. This behavior very likely accounts for some of the drawn out stress–strain behavior found after the stress maximum in the $m = 5$ curves. Ultimately, it is much more difficult to qualitatively observe whether the composite is strong or weak from the pattern of breaks for $m = 5$ than for $m = 10$. Moreover, determining the relative composite strength from the fiber break pattern is generally not a simple task for any value of m.

5.2. Strength distributions

To study size effects in both length, $\hat{L}_T$, and in number of fibers, or bundle size, composite strengths were generated for bundle sizes of 10×10 to 35×35 fibers, and $\hat{L}_T$ ranging from 3 to 12. Each distribution consists of 500 simulation data points, and for a few $m = 10$ cases 1000 simulations, wherein each sample composite was generated from a different random set of segment strengths and

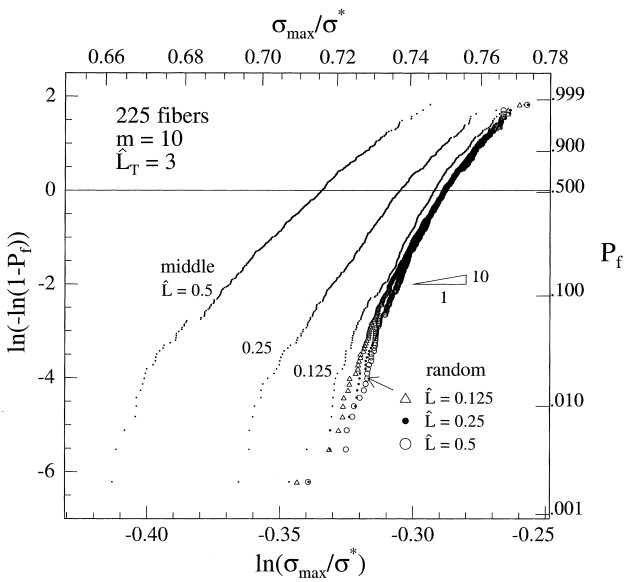

Fig. 8. The strength distributions for a composite with 225 fibers with $m = 10$ and $\hat{L}_T = 3$. There are six strength distributions: three for flaw sites placed in the middle of each segment and three for sites placed randomly within a segment. For each set of three, the normalized segment length was 0.125, 0.25 or 0.5. Notice that the flaws placed randomly within a segment converge faster with respect to decreasing segment length.

flaw locations. To emphasize the difference between the composite strength distribution and that of its fiber reinforcement, all of the distributions are plotted as Weibull probability graphs. These plots relate the fraction P_f of specimens, failing at a stress σ_{max} or less, to the ratio σ_{max}/σ^*. The ordinate is $\ln(-\ln(1-P_f))$ and the abscissa is $\ln(\sigma_{max}/\sigma^*)$. If Eq. (10) were plotted in this way with $\hat{P}_f$ replacing P_f, it would give a straight line with slope m. From any set of 500 simulations, the 500 strengths are ranked in ascending order, $\sigma_{max}^{(i)}$, $i = 1$–500. The P_f associated with $\sigma_{max}^{(i)}$ is then $P_f^{(i)} = i/(500+1)$. Error estimates were carried out for all of the distributions by using confidence interval estimators for normal distributions. In all cases the mean was within 0.1% of the reported mean with 95% confidence, and in many of the plots, this interval is the size of the symbols used to plot each simulation data point in the distributions.

5.3. Failure site discretization study

An initial series of simulations was performed to determine the appropriate choice of the discretization size, $\hat{L}$, and to compare the effects of flaws placed in the middle of a segment to the effects of flaws randomly distributed within the segments. Fig. 8 is a plot of six sets of 500 simulations, each for the cumulative probability vs the ultimate strength of the composite. A small triangle is present on Fig. 8 for comparison, showing the slope of the Weibull strength distribution of the fibers themselves. It can be seen in all cases that the composite material

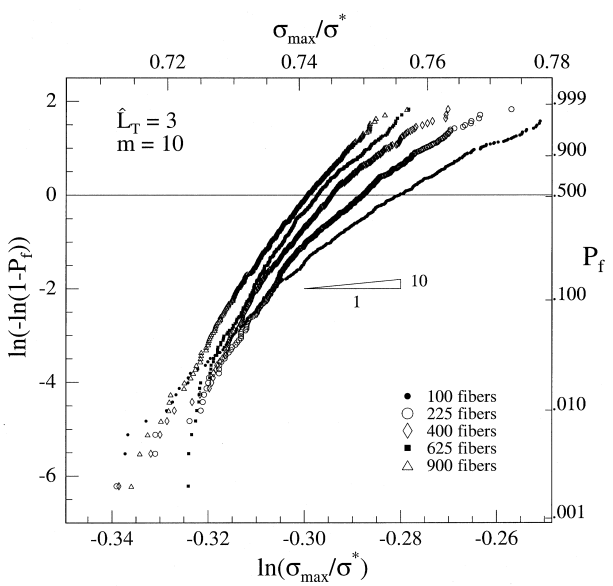

Fig. 9. Strength distributions for composites with $m = 10$ and $\hat{L}_T = 3$ for bundle sizes of 100, 225, 400, 625 and 900 fibers.

exhibits much less strength variability than the isolated fibers. All of the strength distributions on the plot in Fig. 8 are for periodic bundles of 15×15 fibers, with $\hat{L}_T = 3$ and $m = 10$. On this graph three discretization sizes are compared, $\hat{L} = 0.5$, 0.25, and 0.125. Also on Fig. 8 is a comparison of placing the flaws randomly within the segments to placing them in the middle of the segments. It is evident that flaws placed in the middle of the segments yield a low estimate for the strength, whereas random placement of flaws gives a higher estimate. In these cases, flaw placement influences the failure patterns and thus, the ultimate strength. As $\hat{L}$ is decreased, however, both mid-segment and random flaw placements converge to the same strength distribution as seen in Fig. 8. However, random flaw placement provides faster convergence than mid-segment placement. In fact, it is difficult to differentiate between the distributions for $\hat{L} = 0.5$, 0.25, and 0.125 for the randomly placed flaws. For all of the remaining simulations to be discussed, a discretization size of $\hat{L} = 0.25$ was used along with randomly placed flaws.

5.4. Size effects in composite bundle size

Fig. 9 is a plot of the strength distribution on Weibull coordinates for composites with normalized total length $\hat{L}_T = 3$, fiber Weibull modulus $m = 10$ and periodic bundle sizes of 10×10, 15×15, 20×20, 25×25 and 30×30 fibers. Note that there is a consistent size effect for the strength of the composite, except

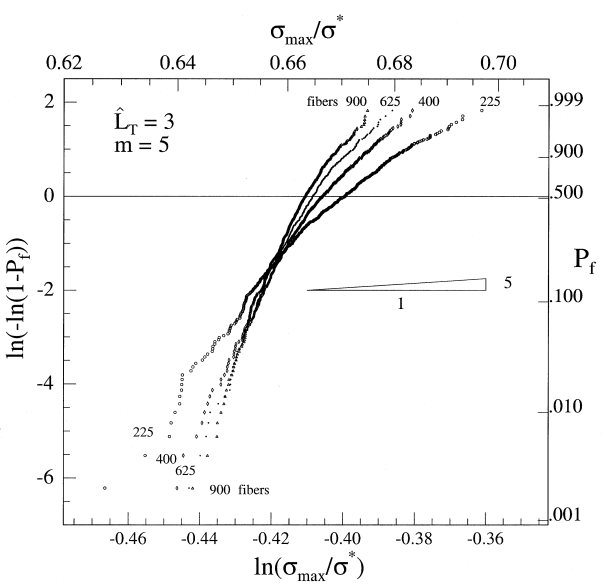

Fig. 10. Strength distributions for composites with $m = 5$ and $\hat{L}_T = 3$ for bundle sizes of 100, 225, 400, 625 and 900 fibers.

when there are 10×10 fibers, i.e. 15×15 fibers is stronger than 20×20 fibers which is stronger than 25×25 fibers and so on for the same probability of failure. For the case of 10×10 fibers the strength distribution crosses over the distributions for larger bundle sizes, i.e. the upper tail of the 10×10 fiber strength distribution is stronger than the upper tail of the larger bundles and its lower tail is weaker than that of the larger bundles. This crossover is due to the higher variability of the strength for the small 10×10 fiber bundle and has been reported in theoretical investigations of finite GLS bundles, Ibnabdeljalil (1994). Overall, the trend is that the variability of the composite strength decreases as the number of fibers in the composite increases.

As in Fig. 9, Fig. 10 contains strength distributions for $\hat{L}_T = 3$, $m = 5$ and periodic bundle sizes of 15×15, 20×20, 25×25 and 30×30 fibers. Again each distribution contains 500 simulations but for higher fiber strength variation, $m = 5$. Note that in this case the distributions cross over one another just as in the case of 10×10 fibers for $m = 10$. For example, for $P_f < 0.10$ the 30×30 fiber bundle is stronger than the 25×25 fiber bundle and so forth. Note that the crossover between two distributions takes place at lower strengths as the number of fibers in the periodic bundle increases. Therefore, it is reasonable to postulate that this crossover behavior will diminish for $m = 5$ as the number of fibers in the periodic bundle is increased. This explanation is supported by the results for the $m = 10$ case shown in Fig. 9, where, for the probability range shown, there is a

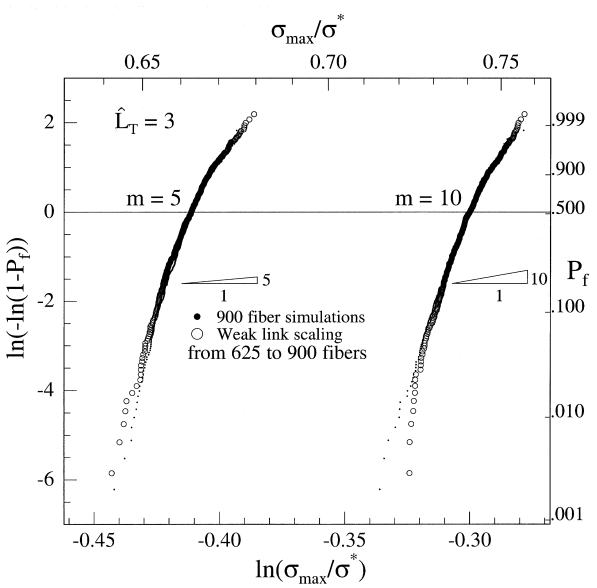

Fig. 11. Comparison of the simulated results for 900 fibers with the results from 625 fibers scaled to 900 fibers using Eq. (14) for $m = 5$ and 10.

crossover between the 10×10 and 15×15 fiber bundles but no crossover occurs between the 30×30 and 25×25 fiber bundles.

If the strength of a material is governed by weak link statistics, then the cumulative probability of failure, P_{f,V_2}, of a composite with volume V_2 loaded to stress σ can be related to the cumulative probability of failure, P_{f,V_1}, of a composite with volume V_1 by

$$P_{f,\,V_2}(\sigma) = 1 - [1 - P_{f,\,V_1}(\sigma)]^{\frac{V_2}{V_1}} \tag{14}$$

where the normalized volume of the composite in our model is given by $V = N^2 \hat{L}_T$. Fig. 11 plots the strength distributions for periodic bundle sizes of 30×30 fibers with $\hat{L}_T = 3$ and $m = 5$ and 10 along with the distributions for bundles of 25×25 fibers with $\hat{L}_T = 3$, $m = 5$ and 10, weak link scaled using Eq. (14) to 30×30 fibers, i.e. with $V_2/V_1 = 900/625$. The plots show that weak link scaling works very well, except at the very lowest strengths, for the parameter values used in these model composites. The weak link scalings for comparing bundles of 20×20 fibers to bundles of 30×30 fibers are not shown on the plots but we mention that these results are not as good as the 25×25 to 30×30 scalings. The bundles of 20×20 fibers underpredict the strength of bundles of 30×30 fibers. Therefore, there is a minimum bundle size for a given m and $\hat{L}_T$, for which weak link scaling, Eq. (14), is valid.

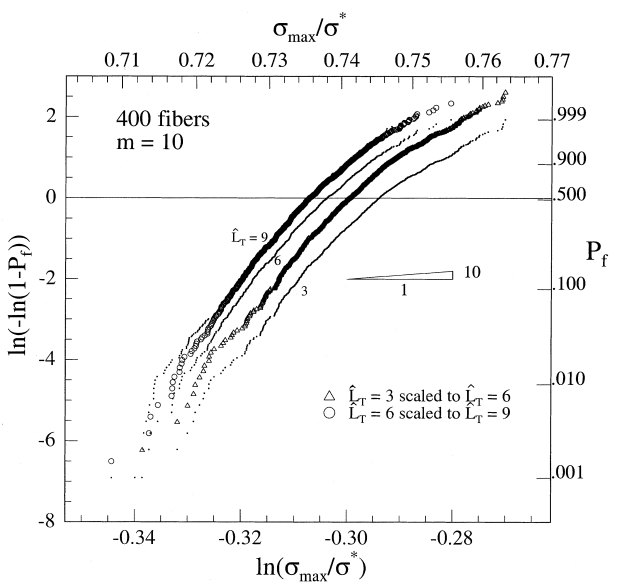

Fig. 12. Strength distributions for composites with 400 fibers and $m = 10$ for normalized composite lengths of 3, 6 and 9. Along with the simulated results are results for $\hat{L}_T = 3$ scaled to 6 and $\hat{L}_T = 6$ scaled to 9 using Eq. (14).

5.5. Size effects in composite length

Fig. 12 is a plot of 5 strength distributions. All of the distributions are for periodic 20 × 20 fiber bundles with $m = 10$. The distributions of black dots are the directly simulated results for normalized damageable lengths of $\hat{L}_T = 3$, 6, and 9. There is a clear decrease in strength as the composite length increases. Also on the figure are two weak linked distributions. The open triangles represent the $\hat{L}_T = 3$ distribution weak link scaled to $\hat{L}_T = 6$. Note that the scaled distribution overpredicts the strength of the larger composite size. Therefore, the composite length $\hat{L}_T = 3$ is not long enough to predict longer composite lengths for 20 × 20 fiber bundles with $m = 10$. On the other hand, the distribution for $\hat{L}_T = 6$ predicts the strength distribution for $\hat{L}_T = 9$ remarkably well after weak link scaling (open circles). Hence, for 20 × 20 fibers with $m = 10$, $\hat{L}_T = 6$ appears to be an adequate normalized length to predict longer composite strengths using weak link scaling. We are careful not to claim that $\hat{L}_T = 6$ is the length that can be used for scaling results for all fiber bundle sizes and Weibull moduli because this is not the case. Calculations identical to those shown in Fig. 12 were done except with bundle sizes of 25 × 25 fibers, $m = 10$ and 20 × 20 fibers, $m = 5$. In these cases both the distributions of $\hat{L}_T = 3$ scaled to $\hat{L}_T = 6$ and $\hat{L}_T = 6$ scaled to $\hat{L}_T = 9$ overpredict the

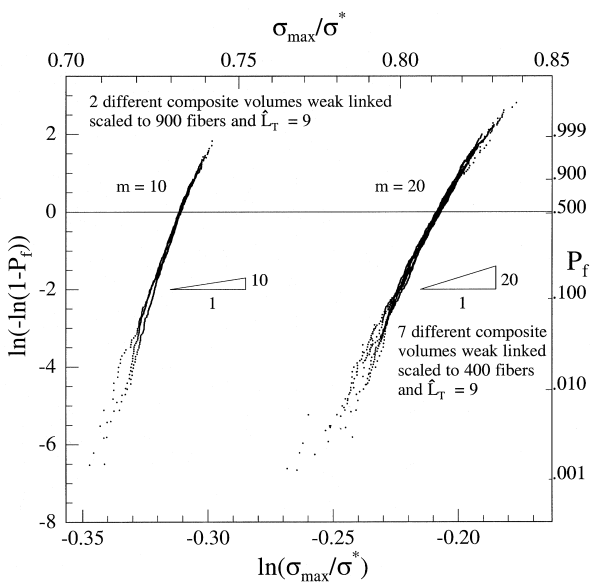

Fig. 13. The minimum weak link scaleable sizes for $m = 10$ and 20. Three distributions for $m = 10$, 900 fibers $\hat{L}_T = 9$, 900 fibers $\hat{L}_T = 12$, and 1225 fibers $\hat{L}_T = 9$, each scaled to the 900 fiber $\hat{L}_T = 9$ size. Seven strength distributions for $m = 20$, 225 fibers $\hat{L}_T = 6$, 225 fibers $\hat{L}_T = 9$, 400 fibers $\hat{L}_T = 6$, 400 fibers $\hat{L}_T = 9$, 625 fibers $\hat{L}_T = 6$, 625 fibers $\hat{L}_T = 9$, and 900 fibers $\hat{L}_T = 6$, each scaled using Eq. (14) to an intermediate normalized volume of 3600 (equal to 400 fibers and $\hat{L}_T = 9$).

strengths of the directly simulated $\hat{L}_T = 6$ and $\hat{L}_T = 9$ distributions respectively. While the lengths that we simulated for these cases were not sufficient to demonstrate weak link scaling, the scaled distributions do become better predictors of the simulated distributions as their length increases. We expect that if longer composites were simulated, eventually a given size would scale to longer composite strength distributions for these bundle sizes and Weibull moduli.

A tentative conclusion from the length scaling results is that the composite length necessary to produce weak link scaling increases as the composite bundle size increases and as the fiber Weibull modulus decreases. Figs. 4 and 5 also lead us to the related conclusion that as m decreases, larger bundle sizes are required to produce weak link scaling. If weak link scaling does hold true for these model composites, then for each value of the fiber Weibull modulus there will exist a fiber bundle size and length that can be used to predict the strengths of larger composites. For Weibull moduli of $m = 5$ and 10 this size is greater than 625 fibers with $\hat{L}_T = 6$.

5.6. Weak link scaling for Weibull modulus m = 10 and 20

In order to support the claim that a "large enough" composite length and number of fibers can be used along with weak link scaling to predict the strengths of larger composites, simulations were done for different composite sizes with $m = 20$ and even larger sizes for $m = 10$. The minimum scaleable size for $m = 5$ was not found due to computational size limitations. If weak link scaling is applicable then there will exist a composite size such that all of the strength distributions of composites with more fibers and longer lengths can be predicted from the distribution of the smaller composite. For $m = 10$ we found that the composite size with 30×30 fibers and $\hat{L}_T = 9$ performed reasonably at predicting the distributions for 35×35 fibers with $\hat{L}_T = 9$ and 30×30 fibers with $\hat{L}_T = 12$. Fig. 13 contains these three distributions each weak link scaled to the 30×30 fiber, $\hat{L}_T = 9$ size.

For $m = 20$ the minimum scaleable size is close to 15×15 fibers and $\hat{L}_T = 6$. Along with the $m = 10$ distributions, Fig. 13 also shows plots of 7 distributions; 15×15 fibers with $\hat{L}_T = 6$; 15×15 fibers with $\hat{L}_T = 9$; 20×20 fibers with $\hat{L}_T = 6$; 20×20 fibers with $\hat{L}_T = 9$; 25×25 fibers with $\hat{L}_T = 6$; 25×25 fibers with $\hat{L}_T = 9$; and 30×30 fibers with $\hat{L}_T = 6$, each scaled using Eq. (14) to an intermediate normalized volume of $V_2 = N^2\ \hat{L}_T = 3600$ (equal to 400 fibers and $\hat{L}_T = 9$). As shown in Fig. 13, it is impossible to differentiate between the distributions except possibly in the lower tails. The approximate error in the mean of these curves to 95% confidence is 0.1% which is about equal to the thickness of the distributions at $P_f = 0.5$. For $m = 20$, smaller composite sizes of 10×10 fibers with $\hat{L}_T = 6$ and 15×15 fibers with $\hat{L}_T = 3$ were also scaled to a volume of 3600 with less success than 15×15 fibers and $\hat{L}_T = 6$. Notably, we also found that the larger bundle sizes, 25×25 and 30×30 fibers, with shorter lengths, $\hat{L}_T = 3$, did not scale to the proper distribution. Therefore, we conclude that for $m = 20$, a composite size of at least 15×15 fibers and length of $\hat{L}_T = 6$ can be used to predict the strength of

composites that are *larger* than a 15×15 array of fibers and *longer* than $\hat{L}_T = 6$. While $m = 20$ is unrealistically high for most fibers, this Weibull modulus was examined to further illustrate that weak link scaling does set in at an appropriate composite size and this size depends on the fiber Weibull modulus.

6. Comparison to experiment

To verify that this model yields reasonable predictions for composite strength we will compare this model to the careful measurements of Bader and Priest (1982). Bader and Priest measured the strength of brittle epoxy impregnated tows made of 1000 carbon fibers as well as the strengths of fibers extracted from similar tows. Later, Padgett et al. (1995) performed maximum likelihood estimates to obtain m, σ_0 and L_0 from the Bader and Priest extracted fiber data. They found that $m \approx 5.3$ and $\sigma_0 \approx 5$ GPa for a gauge length of $L_0 = 1$ mm. The Celion carbon fibers had $E_f \approx 250$ GPa and an average diameter of 8 μm. The shear modulus of the Shell 828 epoxy matrix was 1 GPa. Using these composite properties and scaling our $m = 5$, $\hat{L}_T = 3$, 30×30 fiber simulations to the size of the 1000 fiber 20 mm and 50 mm tows we obtain a median tow strength of 2.96 GPa for both tow sizes. The median tow strengths for the Bader and Priest measurements were 2.82 GPa for the 20 mm tows and 2.81 GPa for the 50 mm tows representing an error of less than 6% between the theory presented here and the experiments. We note, however, that the variability of the strength predicted by our model is significantly lower than that measured in the experiments. This difference suggests that consideration of the variability of the fiber strengths alone is not sufficient for predicting the variability of the composite strength. Other sources of composite variability which may affect the variability of composite strength include variability in fiber spacing, alignment, diameter and initial fiber damage. None of these factors have been included in this model.

7. Discussion and conclusions

In this work we have presented a theoretical model that is able to predict the stress–strain response and statistical strength distributions of an elastic, fiber reinforced composite material. The calculation of the stress distributions in the fibers is carried out by a shear lag model that is based on the finite element method which, in turn, is a reasonable approximation to the exact behavior. By resorting to simplified but reasonable approximations of mechanics as used in this model, we have been able to analyze material system sizes that are orders of magnitude larger than those that can be investigated with more exact methods, e.g. FEA. The system size and local load sharing features of this model have allowed us to examine the effect that composite volume has on strength in these linear elastic composite systems with a well bonded interface. In addition to producing stress–strain curves and strength distributions, this model has allowed

us to closely follow the evolution of damage that occurs in these idealized composites. In some of the simulations, we have been able to directly observe fiber break clustering and propagation, a mechanism of primary importance in determining the strength and reliability of structural composites.

The strength parameter,

$$\sigma^* = \sigma_0 \left(\sqrt{\frac{4}{3\pi}} \sqrt{\frac{G_m}{E_f}} \frac{L_0}{D} \right)^{1/m},$$

is a significant feature of this model. Compare this to

$$\sigma_c = \left(\frac{2\sigma_0^m \tau_0 L_0}{D} \right)^{\frac{1}{m+1}}$$

for GLS strength models. The most significant differences between this strength normalization and the one present in GLS models is the dependence on the elastic properties of the fibers and matrix and the lack of dependence on the fiber/matrix interface sliding stress τ_0. This of course arises due to the fact that in this model, the transfer of loads lost from breaks is controlled by the elasticity of the system while in GLS, load transfer is governed by sliding at the fiber/matrix interface.

For some of the Monte Carlo simulations, the stress–strain behavior of the fiber bundle and the spatial distributions of breaks were studied. We found that the strength of the composite decreases as the Weibull modulus of the fibers decreases (in the range of $5 \leq m \leq 20$), with all other variables being equal. There is much more distributed damage in the composites with $m = 5$ fibers than in composites with $m = 10$ fibers. Due to greater numbers of breaks, the stress–strain behavior in $m = 5$ composites is more compliant than the composites with $m = 10$ or 20 fibers.

As failure progresses under increasing strain and small clusters of breaks form throughout the material, the commonly accepted scenario is that a dominant "critical cluster" of breaks is formed, which causes failure of the rest of the fibers without further increases in composite stress. Qualitatively, it was shown that the weaker simulations from a distribution contained more breaks on the final failure plane just prior to failure than the stronger distributions. In fact, in some weak distributions with 400 and 625 fibers and $m = 10$, a localized crack or dominant cluster of breaks was found prior to failure. However, in the examination of 3-D failure patterns like the ones shown in Figs. 5 and 7, we find more often that a *critical cluster cannot be easily defined*. This was true even in the $m = 10$ and 20 cases where clusters like the ones found in Fig. 4 occur only in the weakest simulations and are the exception rather than the rule. Recall that in these cases, the appropriate volume was found to give weak link scaling.

A question to be addressed was, do composites made from fibers that obey

weak link statistics (WLS) also obey weak link statistics, and if so how large must the composite be for WLS to be valid. The first attempt to find weak link scaling was for composites with fiber Weibull moduli comparable to the fibers used in real composites, $m = 5$ and 10. For these values of m, we found that for a given composite length it was possible to find a large enough fiber bundle size and that for a given bundle size it was possible to find a long enough composite length to yield weak link scaling. However, the strength distribution for a composite with both a minimum bundle size and length is required for accurate prediction of the strength of larger composites. Furthermore, the calculations suggest that the minimum composite length and fiber bundle size needed for weak link scaling increases as the fiber Weibull modulus decreases. The composite size of 30×30 fibers with $\hat{L_T} = 9$ was found to be a likely candidate for the minimum scaleable size for $m = 10$. Also, the composite size of 15×15 fibers and a normalized length of $\hat{L_T} = 6$ was found to scale up to all composite sizes with 15×15 fibers or more *and* a normalized length of six or more for $m = 20$, lending support to the claim that the minimum scaleable volume increases as m decreases.

The work presented here is the first of its kind to solve the governing shear lag equations exactly for arbitrary three dimensional configurations of breaks. Also, a scheme for assigning strengths along a fiber, which allows for larger segment lengths for the same level of accuracy achieved with previous computational models of this kind was introduced. These calculations set a benchmark for comparison of future failure simulations that may potentially include more physical features such as the effects of non-Weibull fiber statistics, non-linear matrix constitutive behavior, axial matrix stiffness, fiber/matrix interface sliding and irregular fiber spacing and alignment which were not included in this model. Finally, the model has proven to be an excellent tool for further investigation of fiber break cluster formation and propagation.

Acknowledgements

CML and RMM were supported by the Advanced Research Projects Agency through the University Research Initiative at the University of California, Santa Barbara (ONR Contract N-0014-92-J-1808). CML was also supported by a Regents Fellowship from the University of California. IJB is grateful for the support provided at Los Alamos National Laboratory under a J. R. Oppenheimer Postdoctoral Fellowship.

Appendix A

In this appendix we will outline the solution procedure to the set of equations given by Eq. (1). The solution requires the characterization of the eigensystem of the appropriate matrix. Eq. (1) can be written as

$$\frac{\mathrm{d}^2}{\mathrm{d}\xi^{\ast 2}}\begin{Bmatrix} u_{0,\,0} \\ u_{0,\,1} \\ u_{0,\,2} \\ \vdots \\ u_{N-1,\,N-1} \end{Bmatrix} + \begin{bmatrix} A_{0000} & A_{0001} & A_{0002} & \cdots & A_{00(N-1)(N-1)} & \\ & A_{0101} & A_{0102} & \cdots & A_{01(N-1)(N-1)} & \\ & & A_{0202} & \cdots & A_{02(N-1)(N-1)} & \\ & \text{sym} & & \ddots & \vdots & \\ & & & & & A_{(N-1)(N-1)(N-1)(N-1)} \end{bmatrix} \times \begin{Bmatrix} u_{0,\,0} \\ u_{0,\,1} \\ u_{0,\,2} \\ \vdots \\ u_{N-1,\,N-1} \end{Bmatrix} = 0 \tag{15}$$

where the only non-zero A_{ijkl} are

if $0 \le i \le N-1$

and $0 \le j \le N-1$

$A_{ijij} = -8$

$A_{ij(i-1)j} = 1$

$A_{ij(i+1)j} = 1$

$A_{iji(\,j-1)} = 1$

$A_{iji(\,j+1)} = 1$

$A_{ij(i-1)(\,j-1)} = 1$

$A_{ij(i-1)(\,j+1)} = 1$

$A_{ij(i+1)(\,j-1)} = 1$

$$A_{ij(i+1)(j+1)} = 1 \tag{16a–i}$$

Note that $A_{ijkl} = A_{klij}$. Due to the periodic boundary conditions if $i = 0$ or $j = 0$ then the subscripts $(i-1)$ or $(j-1)$ become $(N-1)$, and if $i = N-1$ or $j = N-1$ then the subscripts $(i+1)$ or $(j+1)$ become 0. We need to find the eigenvalues, λ_{ij}^2, and eigenvectors, C_{ijkl}, of the matrix $[-\mathbf{A}]$. The minus sign appears in order to make all of the eigenvalues positive. The eigenvalues and the components of the un-normalized eigenvectors are determined using the *tred2* and *tqli* subroutines from *Numerical Recipes* (Press et al., 1992). The components of the eigenvectors must satisfy the following conditions:

$$\sum_{k=0}^{N-1}\sum_{l=1}^{N-1} -\lambda_{kl} C_{00kl} = -1$$

$$\sum_{k=0}^{N-1}\sum_{l=0}^{N-1} C_{ijkl} = 0 \quad \text{for all } ij \neq 00 \tag{17a,b}$$

such that the boundary conditions for a unit opening load, i.e.

$$\frac{\mathrm{d}u_{0,\,0}}{\mathrm{d}\xi}(\xi = 0) = -1$$

$$u_{m,\,n}(\xi = 0) = 0 \quad \text{for all } (m, n) \neq (0, 0)$$

$$\frac{\mathrm{d}u_{m,\,n}}{\mathrm{d}\xi}(\xi = \infty) = 0 \quad \text{for all } m \text{ amd } n \tag{18a–c}$$

are satisfied.

Once the C_{ijkl} are determined the solution for the fiber displacements is

$$u_{m,\,n} = \sum_{i=0}^{N-1}\sum_{j=0}^{N-1} C_{mnij}\ \exp[-\lambda_{ij}\xi] \tag{19}$$

the influence functions are

$$q_{m,\,n} = \sum_{i=0}^{N-1}\sum_{j=0}^{N-1} -\lambda_{ij} C_{mnij}\ \exp[-\lambda_{ij}\xi] \tag{20}$$

and the crack opening displacement is

$$u^{\mathrm{open}} = 2u_{0,\,0}(\xi = 0) = 2\sum_{i=0}^{N-1}\sum_{j=0}^{N-1} C_{00ij}. \tag{21}$$

References

Bader, M.G., Priest, A.M., 1982. Statistical aspects of fibre and bundle strength in hybrid composites. In: Hayashi, T., Kawata, K., Umekawa, S. (Eds.), Progress in Science and Engineering Composites, pp. 1129–1136 ICCM-IV.

Beyerlein, I.J., Landis, C.M., 1999. Shear-lag model for failure simulations of unidirectional fiber composites including matrix stiffness. Mechanics of Materials 31, 331–350.

Beyerlein, I.J., Phoenix, S.L., 1996. Stress concentrations around multiple fiber breaks in an elastic matrix with local yielding or debonding using quadratic influence superposition. J. Mech. Phys. Solids 44, 1997–2039.

Beyerlein, I.J., Phoenix, S.L., 1997a. Statistics of fracture for an elastic notched composite lamina containing Weibull fibers — Part I. Features from Monte-Carlo simulation. Eng. Frac. Mech. 57, 241–265.

Beyerlein, I.J., Phoenix, S.L., 1997b. Statistics of fracture for an elastic notched composite lamina containing Weibull fibers — Part II. Probability models of crack growth. Eng. Frac. Mech. 57, 267–299.

Beyerlein, I.J., Phoenix, S.L., Raj, R., 1998. Time evolution of stress redistribution around multiple fiber breaks in a composite with viscous and viscoelastic matrices. Int. J. Solids Structures 24, 3177–3211.

Curtin, W.A., 1991a. Theory of mechanical properties of ceramic matrix composites. J. Am. Ceram. Soc. 74, 2837–2845.

Curtin, W.A., 1991b. Exact theory of fiber fragmentation in a single filament composite. J. Mater. Sci. 26, 5239–5253.

Harlow, D.G., Phoenix, S.L., 1978a. The chain-of bundles probability model for the strength of fibrous materials I: analysis and conjectures. J. Comp. Mat. 12, 195–214.

Harlow, D.G., Phoenix, S.L., 1978b. The chain-of bundles probability model for the strength of fibrous materials II: a numerical study of convergence. J. Comp. Mat. 12, 314–334.

Hedgepeth, J.M., 1961. Stress concentrations in filamentary structures. NASA TN D-882.

Hui, C-Y., Phoenix, S.L., Ibnabdeljalil, M., 1995. An exact closed form solution for fragmentation of Weibull fibers in a single filament composite with applications to fiber-reinforced ceramics. J. Mech. Phys. Solids 43, 1551–1585.

Ibnabdeljalil, M., 1994. Statistical aspects of the failure of brittle matrix composites, reinforced with unidirectional continuous, discontinuous and time dependent brittle fibers. Ph.D. Thesis, Department of Theoretical and Applied Mechanics, Cornell University.

Ibnabdeljalil, M., Curtin, W.A., 1997. Strength and reliability of fiber-reinforced composites: localized load-sharing and associated size effects. Int. J. Solids Structures 34, 2649–2668.

Landis, C.M., McGlockton, M.A., McMeeking, R.M., 1999. An improved shear lag model for broken fibers in composites. J. Comp. Mat. 33, 667–680.

Landis, C.M., McMeeking, R.M., 1999. Stress concentrations in composites with interface sliding, matrix stiffness, and uneven fiber spacing using shear lag theory. Int. J. Solids Structures 36, 4333–4361.

Nedele, M.R., Wisnom, M.R., 1994. Three-dimensional finite element analysis of the stress concentration at a single fibre break. Comp. Sci. Technol. 51, 517–524.

Neumeister, J.M., 1993. A constitutive law for continuous fiber reinforced brittle matrix composites with fiber fragmentation and stress recovery. J. Mech. Phys. Solids 41, 1383–1404.

Padgett, W.J., Durham, S.D., Mason, A.M., 1995. Weibull analysis of the strength of carbon fibers using linear and power law models for the length effect. J. Comp. Mat. 29, 1873–1884.

Phoenix, S.L., Ibnabdeljalil, M., Hui, C-Y., 1997. Size effects in the distribution for strength of brittle matrix fibrous composites. Int. J. Solids Structures 34, 545–568.

Press, W.H., Teukolsky, S.A., Vettering, W.T., Flannery, B.P., 1992. Numerical Recipes in Fortran, 2nd ed. Cambridge University Press, pp. 779–783.

Sastry, A.M., Phoenix, S.L., 1993. Load redistribution near non-aligned fiber breaks in a two dimen-

sional unidirectional composite using break influence superposition. J. Mater. Sci. Lett. 12, 1596–1599.

Van den Heuvel, P.W.J., Van der Bruggen, Y.J.W., Peijs, T., 1996. Failure phenomena in multi-fiber model composites. 1. An experimental investigation into the influence of fibre spacing and fibre-matrix adhesion. Composites 27A, 855–859.

Zhou, S.J., Curtin, W.A., 1995. Failure of fiber composites: A lattice Green function model. Acta Metall. Mater 43, 3093–3104.